

Scientific Article

Internal Target Volume Estimation for Liver Cancer Radiation Therapy Using an Ultra Quality 4-Dimensional Magnetic Resonance Imaging



Yen-Peng Liao, PhD,^a Haonan Xiao, PhD,^{b,c} Peilin Wang, MSc,^b Tian Li, PhD,^b Todd A. Aguilera, MD, PhD,^a Justin D. Visak, PhD,^a Andrew R. Godley, PhD,^a You Zhang, PhD,^a Jing Cai, PhD,^b and Jie Deng, PhD^{a,*}

^aDepartment of Radiation Oncology, UT Southwestern Medical Center, Dallas, Texas; ^bDepartment of Health Technology and Informatics, The Hong Kong Polytechnic University, Hong Kong, China; and ^cDepartment of Radiation Physics, Shandong Cancer Hospital, Shandong, China

Received 6 January 2025; accepted 21 March 2025

Purpose: Accurate internal target volume (ITV) estimation is essential for effective and safe radiation therapy in liver cancer. This study evaluates the clinical value of an ultraquality 4-dimensional magnetic resonance imaging (UQ 4D-MRI) technique for ITV estimation.

Methods and Materials: The UQ 4D-MRI technique maps motion information from a low spatial resolution dynamic volumetric MRI onto a high-resolution 3-dimensional MRI used for radiation treatment planning. It was validated using a motion phantom and data from 13 patients with liver cancer. ITV generated from UQ 4D-MRI (ITV_{4D}) was compared with those obtained through isotropic expansions (ITV_{2 mm} and ITV_{5 mm}) and those measured using conventional 4D-computed tomography (computed tomography-based ITV, ITV_{CT}) for each patient.

Results: Phantom studies showed a displacement measurement difference of <5% between UQ 4D-MRI and single-slice 2-dimensional cine MRI. In patient studies, the maximum superior-inferior displacements of the tumor on UQ 4D-MRI showed no significant difference compared with single-slice 2-dimensional cine imaging (P = .985). Computed tomography-based ITV showed no significant difference (P = .72) with ITV_{4D}, whereas ITV_{2 mm} and ITV_{5 mm} significantly overestimated the volume by 29.0% (P = .002) and 120.7% (P < .001) compared with ITV_{4D}, respectively.

Conclusions: UQ 4D-MRI enables accurate motion assessment for liver tumors, facilitating precise ITV delineation for radiation treatment planning. Despite uncertainties from artificial intelligence-based delineation and variations in patients' respiratory patterns, UQ 4D-MRI excels at capturing tumor motion trajectories, potentially improving treatment planning accuracy and reducing margins in liver cancer radiation therapy.

© 2025 The Author(s). Published by Elsevier Inc. on behalf of American Society for Radiation Oncology. This is an open access article under the CC BY-NC-ND license (http://creativecommons.org/licenses/by-nc-nd/4.0/).

Sources of support: General Research Fund (GRF 15104822, 15102219, and 15104323), the University Grants Committee; Health and Medical Research Fund (HMRF 10211606), the Health Bureau; Innovation and Technology Support Programme (ITS/049/22FP), Innovation and Technology Commission, Hong Kong Special Administrative Regions.

The clinical data used in this study are not publicly available because of institutional policies and patient confidentiality. However, reasonable

requests for data access can be directed to the corresponding author, subject to approval by our institution and compliance with ethical guidelines.

*Corresponding author: Jie Deng, PhD.; Email: jie. deng@utsouthwestern.edu

Introduction

Radiation therapy (RT) is one of the primary strategies for treating liver cancer, offering a noninvasive alternative to surgical intervention, particularly an approach known as stereotactic body RT.¹ Based on image guidance, it allows for precise deposition of highly focused and destructive doses of radiation, enhancing local tumor control while minimizing damage to surrounding normal tissue. RT planning requires information from computed tomography (CT) and/or magnetic resonance imaging (MRI), known as CT-simulation (CT-Sim) and MR-simulation (MR-Sim), to provide accurate tumor delineation.²

Based on CT- or MR-Sim images, oncologists contour the gross tumor volume (GTV) and then add a margin along 3 directions to estimate invisible disease spread to form the clinical target volume (CTV). Respiratory-induced tumor motion is then included to form the internal target volume (ITV) from the CTV, and lastly, systematic and random changes during radiation delivery are included to form the planning target volume (PTV).3 Accurate definition of ITV is crucial not only for ensuring adequate target coverage but also for minimizing radiation exposure to surrounding normal tissues, such as liver parenchyma, stomach, duodenum, and bowels. Reducing exposure to these critical structures may enable dose escalation while maintaining organ at risk constraints, potentially improving treatment efficacy. For a small metastatic liver tumor (<1 cm) that is poorly visualized on CT- or MR-Sim images, a large margin (5 mm to 2 cm) is commonly added.4-7 This margin region of normal tissue receives the prescription dose yielding a significant toxicity concern.

Respiratory motion is a main source of targeting uncertainty in radiation dose delivery to liver tumors. Several approaches have been used to reduce the impact of motion, such as using a compression of the patient's abdomen⁸ and breath-hold or gated treatment. Motion-resolved 4-dimensional (4D) CT images are taken with respiratory signal and processed to generate volumetric CT images in 10 breathing phases to estimate the range of tumor movement.⁹ Accurate assessment and management of target motion defines the ITV. However, defining ITV from CT images is challenging because of poor tumor-to-liver contrast, even with the use of contrast agents. In addition, acquiring the 4D CT images increases imaging dose to patients.¹⁰

MRI provides versatile tumor-to-liver contrast compared with CT for better liver tumor delineation. Most liver tumors show isointense or hypointense in contrast with liver parenchyma on T1-weighted (T1w) and T2-weighted (T2w) images. The appearance of liver tumors becomes more complicated in diffuse liver diseases with the presence of fat, iron, inflammation, fibrosis, and cirrhosis, in which case a multiphase contrast-enhanced MRI is acquired to provide pharmacokinetic information during arterial, venous, and delay phases. 4D-MRI has been proposed to provide organ motion information. The 4D-MRI methods could

be generally classified as retrospective and prospective techniques. Retrospective methods acquire image data together with respiratory signals such as bellows or image-based navigators, and the signal will be divided into several phase bins afterward. 17-20 For prospective methods, the acquisition is monitored with respiratory signals and ensures the images are acquired at the desired position and phases. 21,22 Both techniques successfully obtained multiple contrasts, including T2/T1w, T2w images, and diffusion-weighted imaging. 13,14,20,22 However, these methods are sensitive to stitching artifacts shown as broken organ boundaries because of irregular breathing and require a long acquisition time. Additionally, most 4D-MRI techniques require specially designed MR (magnetic resonance) sequences with sparsely undersampling acquisition strategies and complicated algorithms to reconstruct a series of temporally resolved high-resolution images. These requirements have greatly hindered the clinical implementation of 4D-MRI.

Model-based 4D-MRI techniques use motion modeling and principal component analysis to extract major motion components. Fast cine MRI is acquired to derive the major motion components, which is used to deform a prior 3dimensional MRI using deformable image registration, 23-26 yet the resulting image contrast is usually limited. More recently, deep learning model-based 4D-MRI reconstruction methods have been developed to generate respiratory phasesorted MR images with multiple image contrasts.²⁷⁻²⁹ One method developed a dual-supervised deformation estimation model to obtain a 4D deformation vector field (DVF) from a low spatial resolution dynamic volumetric MRI scan and then deformed high spatial resolution 3-dimensional MR images using this 4D DVF to generate ultraquality (UQ) 4D-MRI.³⁰ The 3-dimensional MR images can be acquired using any clinically available MRI sequences (eg, T1w, T2w, or dynamic contrast-enhanced images). This retrospective solution of UQ 4D-MRI with flexibility in image contrast can be easily implemented in clinical settings without any need for specialized research MRI sequences or hardware.

This study evaluated the performance of the UQ 4D-MRI method using a motion phantom and clinical liver cancer cases, demonstrating strong agreement with the existing clinical approach of using 4D CT. We added only a 1-minute low spatial resolution dynamic volumetric MRI scan to our clinical MR-Sim protocol to achieve the 4D-MRI capability for target motion assessment and ITV delineation, offering the potential to reduce margins and streamline RT planning in patients with liver cancer.

Methods and Materials

Phantom study

A ZEUS MR-guided-RT motion phantom (Model 008z, Sun Nuclear) with an insert containing a moving

target was used to simulate respiratory motion. The phantom was driven with superior-inferior (S-I) direction cosine waveforms to create peak-to-peak displacement of 10, 20, and 30 mm (corresponding to amplitudes of 5, 10, and 15 mm) with various periods (4, 6, 8, and 12 seconds). Under each testing condition, axial 3-dimensional T2w and 4D T1w high-resolution isotropic volume examination (THRIVE) images covering the moving target were acquired. A single-slice single-shot balanced fastfield echo (bFFE) sequence was also acquired in a coronal plane at the center of the moving target, serving as the reference for image-based motion measurement along the S-I direction. The peak-to-peak displacements measured on both bFFE and 4D THRIVE image sets were compared under each testing condition to evaluate the accuracy of motion detection.

MR-Sim and CT-Sim imaging protocols

MR-Sim and CT-Sim examinations were performed on patients diagnosed with liver neoplasms receiving RT in our department. During both simulation examinations, an abdominal compression pad was used to limit diaphragmatic displacement. The compression is replicated at each RT session to ensure accurate delivery of radiation to the tumor. As part of our standard of care protocol,

MR-Sim was performed on a clinical 1.5-T MRI scanner (Ingenia Ambition X, Philips Medical Systems), and multiple 3-dimensional sequences were acquired to provide high spatial resolution images with various tumor-to-liver contrast using the parameters listed in Table 1. In addition, a low spatial resolution 4D THRIVE sequence with an isotropic voxel size of $3.0 \times 3.0 \times 3.0 \,\mathrm{mm^3}$ and a temporal resolution of 0.7 seconds were acquired to extract the respiratory motion of the tumor over 1 minute. Additionally, single-slice 2-dimensional cine bFFE imaging with high temporal resolution (0.2 seconds) centered on the tumor area along the coronal and sagittal planes was acquired. The imaging parameters of these motion assessment sequences are listed in Table 2.

To ensure spatial accuracy, our MRI scanner undergoes comprehensive quality assurance testing. The same motion phantom used in this study is employed in annual quality assurance testing to verify the geometric fidelity of dynamic imaging. Additionally, geometric distortion for 3-dimensional sequences used for treatment planning is routinely evaluated through weekly and monthly quality assurance procedures, following the American College of Radiology (ACR) and the American Association of Physicists in Medicine Task Group Report 284 (AAPM TG-284) guidelines.³¹

For CT-Sim, patients underwent 2 types of CT scans in the treatment position. A free-breathing 3-dimensional

Table 1 Magnetic resonance imaging acquisition parameters for 3 clinical sequences: T2w 3-dimensional, T2w SPIR 3-dimensional, and T1w 3-dimensional with/without contrast enhancement.

	T2w 3-dimensional	T2w SPIR 3-dimensional	T1w 3-dimensional with/without contrast	
Contrast-enhanced	No	No	Yes/No	
Acquisition mode	Bellow gating	Bellow gating	None	
Sequence	TSE MultiVane	TSE MultiVane	SoS Vane	
No. of slices	120	95	78	
Slice thickness (mm)	3	3	3	
Fat suppression	No	Yes	No	
Turbo factor	50	39	44	
Flip angle (°)	90	90	10	
Parallel imaging (factor)	SENSE (1.8)	SENSE (1.8)	SENSE (1.8)	
Partial Fourier	N/A	N/A	N/A	
TR (ms)	9586	5227	6.3	
TE (ms)	100	70	1.77/3.7	
Bandwidth (Hz/pixel)	545	629	545	
Acquisition matrix size	$300\times300\times120$	$300 \times 300 \times 95$	$376 \times 376 \times 78$	
Pixel size (mm ²)	1.5×1.5	1.5×1.5	1.2×1.2	
Acquisition time (min:s)	5:16	5:53	3:38	

Abbreviations: SENSE = sensitivity encoding; SoS = stack of stars; SPIR = spectral presaturation with inversion recovery; T1w = T1-weighted; T2w = T2-weighted; TE = echo time; TR = repetition time; TSE = turbo spin echo.

Table 2 Acquisition parameters of real-time MRI acquired during free breathing. Four-dimensional -THRIVE is used for generating ultraquality MRI, and bFFE is used as reference standard.

	4D-THRIVE	bFFE
Contrast-enhanced	No	No
Acquisition mode	Free breathing	Free breathing
No. of slices	53	1
Slice thickness (mm)	3.0	5.0
Fat suppression	SPIR	No
Turbo factor	45	48
Flip angle (°)	10	40
Parallel imaging (factor)	CS-SENSE (9)	SENSE (1.8)
Partial Fourier	0.625(Y)/0.8(Z)	N/A
TR (ms)	3.5	3.7
TE (ms)	1.57	1.61
Bandwidth (Hz/pixel)	499	1076
Acquisition matrix size	$140\times140\times53$	$144 \times 144 \times 1$
Pixel size (mm ²)	0.875×0.875	1.1×1.1
Temporal resolution (s)	0.694	0.198
No. of Frame	87	300
Acquisition time (min:s)	1:04	1:00

Abbreviations: 4D-THRIVE = T1w high-resolution isotropic volume examination; bFFE = balanced fast-field echo; CS-SENSE = compressed sensing with sensitivity encoding; MRI = magnetic resonance imaging.

CT scan with 2-mm slice thickness was first acquired followed by a respiratory-correlated 4D-CT with 10 respiratory phases using bellows monitoring after injecting contrast agent. The key acquisition parameters of 4D-CT include: 120 kV, 600 mAs, 2-mm slice thickness, and 0.059 pitch. From this 4D-CT data set, 2 additional image sets were derived as follows: a maximum intensity projection (MIP) image set for visualizing the full range of respiratory motion and an averaged image set. In the clinical workflow, 3 respiratory phases (0%, 50%, and 90%) from the 4D-CT are selected and imported into the treatment planning system, along with the derived MIP and averaged CT data sets for ITV estimation and treatment planning.

UQ 4D-MRI postprocessing

A liver dome-based sorting method, as proposed by Yang et al,¹⁷ was first applied to the real-time 4D THRIVE images. During the 1-minute real-time acquisition, a total of 87 volumetric images were acquired with a temporal resolution of 0.694 seconds. These images were then sorted into 10 respiratory bins based on the liver dome position, representing different phases of the breathing cycle. A nonlinear curve fitting was then performed on the sorted data to model the respiratory motion. Among all the image

volumes falling into each of the 10 bins, we selected the image volume closest to the fitted curve. These 10 selected image volumes were then used to reconstruct the 4D MRI series, ensuring a representation of the full respiratory cycle while minimizing the impact of any irregularity in the breathing pattern. Then, an automatic selection method was implemented to identify 1 of the 10 selected image volumes with the highest spatial similarity to an arbitrary 3-dimensional MRI by cross-correlation. The 3-dimensional MR image (either T1w, T2w, or contrast-enhanced T1w) was coregistered to the selected image volume of the 4D-THRIVE set using the Elastix software tool (https://github. com/raacampbell/matlab_elastix). The coregistration process involved hierarchical steps, including rigid, affine, and nonrigid B-spline transformations to tackle deformations from coarse to fine. The normalized correlation coefficient served as the cost function for registration, as detailed in Mengler et al's³² study. Subsequently, the other 9 image volumes of 4D-THRIVE were aligned with the selected image volume via a dual-supervised deformation estimation model to generate the DVFs of each phase. These DVFs were then applied to the 3-dimensional MR images to generate UQ 4D-MRI in corresponding phases, resulting in a 10-phase 3dimensional high-resolution MR image series, which can be of any 3-dimensional MRI treatment planning images chosen by the user. From the UQ 4D-MRI series, 2 types of projections were generated as follows: MIP and minimum

intensity projection image sets. For hyperintense tumors relative to the liver parenchyma, the MIP images were used for ITV delineation, whereas minimum intensity projection images were used for hypointense tumors.

Patient data analysis

The retrospective study, exempt from institutional review board review, analyzed 15 liver tumors from 13 patients (7 women; 6 men; mean age, 63.5 years; range, 45-78 years) treated with RT at our institution between October 2023 and January 2024. To validate motion assessment accuracy, the respiratory motion was measured using both single-slice 2-dimensional bFFE imaging and UQ 4D-MRI for each patient. The full S-I displacement was calculated as the difference between the highest and lowest positions of either the liver dome or the tumor during the acquisition period. The S-I sisplacements measured by real-time 2dimensional bFFE imaging (S-I_{bFFE}) were compared with those obtained from UQ 4D-MRI (S-I displacements measured by UQ 4D-MRI) using the paired t test. UQ 4D-MRI data sets (10 phases) were imported into the treatment planning system (Aria-Eclipse, Varian Medical Systems) and fused with other MR-Sim image series. The GTV for each patient was manually contoured by attending radiation oncologists on an 3-dimensional MRI sequence showing optimal image contrast for tumor delineation and served as the basis for generating ITV. The GTV was propagated to either MIP (for hyperintense tumors) or minimum intensity projection (for hypointense tumors) for initial motion envelope assessment. This projection-based contour underwent comprehensive verification and refinement across all 10 respiratory phases, with the final ITV_{4D} generated by combining the verified phase-specific contours to encompass the complete tumor motion trajectory. The ITV_{4D} was then expanded to form the PTV, ensuring adequate coverage for potential tumor motion during treatment with the following steps. Additionally, 2 margin-based ITVs were generated with uniform expansions of the reference GTV: ITV2 mm and ITV_{5 mm} using 2 and 5 mm margins, respectively.

Compared with current clinical practice, the CT-based ITV (ITV $_{\rm CT}$) was generated from the 3 phases (0%, 50%, and 90%) of 4D-CT, along with conventional 3-dimensional CT (with or without contrast). For tumors visible on any of the CT images, the ITV $_{\rm CT}$ was delineated using the 3-phase 4D-CT images by the radiation oncologist. For tumors not visible on CT, the GTV was first contoured on the 3-dimensional-MRI and then fused with the CT images. The ITV $_{\rm CT}$ in these cases was estimated based on the patient's breathing pattern, as inferred from nearby anatomic structures, such as the diaphragm or large vessels, guided by the physician's empirical experience. The volumes of ITVs generated by different approaches (ITV $_{\rm 4D}$, ITV $_{\rm 2~mm}$, ITV $_{\rm 5~mm}$, and ITV $_{\rm CT}$) were compared using the paired t test.

The CT acquisition used an external bellows system, whereas the MRI approach tracked the liver dome as an internal surrogate based on dynamic images. Despite these methodological differences in phase selection and respiratory monitoring, both approaches were designed to capture the full range of respiratory motion under the same abdominal compression setup. Therefore, we hypothesized that the overall motion space and the resulting ITV should be comparable between the 2 methods, regardless of the number of phases used for ITV contour delineation or the type of surrogate signal employed for respiratory monitoring.

Results

Phantom study

The phantom study demonstrated high accuracy of motion measurements using both bFFE and 4D THRIVE sequences under various respiratory periods (4, 6, 8, and 12 seconds) with a peak-to-peak displacement of 10, 20, and 30 mm (Table E1). Notably, the bFFE sequence showed excellent agreement with the preset phantom motion values, with average measured displacements of 10.2, 20.2, and 29.0 mm for the 10, 20, and 30 mm settings, respectively. These results validated bFFE as a reliable gold standard for MRI-based motion measurements. The phantom study tested these displacement ranges to evaluate the 4D THRIVE sequence's capability in capturing motion trajectories across and beyond typical clinical ranges. The results demonstrated that 4D THRIVE maintained reliable motion tracking even at larger displacements. For smaller displacements, the measurement accuracy was fundamentally limited by the 3-mm slice thickness of 4D THRIVE, which should be considered when interpreting the motion range <3 mm. The phantom study demonstrated slight systematic differences (<8%) between bFFE and 4D THRIVE measurements. For the smallest peak-to-peak displacement (10 mm), 4D THRIVE consistently measured 9.0 mm across all respiratory periods, which can be attributed to its 3.0-mm slice thickness, because the displacement can only be captured in multiples of the slice thickness. In contrast, bFFE sequence, acquired as a single coronal slice with higher spatial resolution $(1.1 \times 1.1 \text{ mm}^2)$, provided more precise measurements closer to the expected values.

Patient study

Table 3 shows the comparison of respiratory displacement in the S-I direction between bFFE and UQ 4D MRI and ITV measurements obtained using different approaches in 15 liver tumors from 13 patients. The maximum S-I displacements measured by bFFE (S-

Table 3 Comparison of respiratory displacement (cm) in the S-I direction and ITV measurements (cm 3) by different methods (ITV $_{4D}$, ITV $_{CT}$, ITV $_{2\ mm}$, and ITV $_{5\ mm}$) in 15 liver tumors from 13 patients (Patients 2 and 3 have 2 liver tumors). Different MRI sequences (T2w, T2w SPIR, post-T1w 20 s, post-T1w 90 s) are used in different patients to delineate GTV and to generate ultraquality 4-dimensional magnetic resonance imaging. *P*-value < .05 indicating significant differences.

Patient	Sequence	S-I _{bFFE}	S-I _{UQ4D}	GTV	$\mathrm{ITV_{4D}}$	ITV _{CT}	ITV _{2 mm}	ITV _{5 mm}
1	SPIR	0.45	0.56	25.9	31.4	30.6	40.0	62.1
2	T2w	0.34	0.68	12.0	15.2	15.0	21.8	36.5
				2.0	3.5	3.8	5.0	10.9
3	Post 20 s	0.34	0.32	2.8	3.2	5.6	6.4	13.2
				6.4	7.1	6.1	12.0	21.5
4	T2w	0.34	0.37	15.8	17.1	17.4	25.0	40.0
5	T2w	0.56	0.69	2.9	2.9	2.7	6.2	12.7
6	T2w	0.80	0.82	31.1	55.5	54.8	48.1	73.5
7	SPIR	0.57	0.48	8.9	9.8	3.6	15.9	28.6
8	T2w	0.30	0.34	4.4	4.7	5.8	8.7	16.5
9	SPIR	0.45	0.35	10.2	14.1	12.0	18.2	31.5
10	Post 90 s	0.34	0.31	6.1	6.1	9.2	11.6	21.3
11	SPIR	0.80	0.41	6.6	10.0	9.3	12.6	23.1
12	SPIR	0.60	0.61	4.0	5.9	6.1	7.9	15.8
13	T2w	0.80	0.80	1.6	2.5	4.0	4.4	9.9
Difference (%)					Ref	-1.6	29.0	120.7
P-value		.985				.72	.002	<.0001

Abbreviations: GTV = gross tumor volume; ITV = internal target volume; ITV $_{CT}$ = CT-based ITV; MRI = magnetic resonance imaging; S-I = superior-inferior; S-I $_{UQ4D}$ = S-I displacements measured by UQ 4D-MRI; SPIR = spectral presaturation with inversion recovery; T1w = T1-weighted; T2w = T2-weighted.

 I_{bFFE}) and UQ 4D-MRI (S- I_{UQ4D}) were highly consistent (P=.985), demonstrating the accuracy of motion detection with UQ 4D-MRI. Furthermore, using the ITV derived from UQ 4D-MRI (ITV_{4D}) as the reference, ITV_{CT} showed no significant volumetric difference (mean difference, -1.6%; P=.72). In contrast, ITV_{2 mm} and ITV_{5 mm} significantly overestimated target volumes, with mean differences of 29.0% (P=.002) and 120.7% (P<.0001), respectively.

Figure 1 shows the coronal views of bFFE, 4D THRIVE, and UQ 4D-MRI images (T1w, T2w, and T2 spectral presaturation with inversion recovery [SPIR]) at the same phase of the respiratory cycle for 3 representative patients. The reformatted UQ 4D-MRI in the coronal plane integrates motion information extracted from 4D THRIVE. Compared with 4D THRIVE, UQ 4D-MRI provides high-resolution images, and compared with bFFE, it offers enhanced image quality, both essential for deriving precise ITV based on MRI. The S-I directional motion of the upper and lower margins of the liver/tumor showed high consistency across bFFE, 4D THRIVE, and UQ 4D-MRI images.

Figures 2 to 4 show the comparison of $\mathrm{ITV}_{4\mathrm{D}}$ delineation with $\mathrm{ITV}_{\mathrm{CT}}$ in 3 representative patients. In Fig. 2, both T2w UQ 4D-MRI and 4D CT yielded similar

volumes (17.1 vs 17.4 cm³) but showed distinct motion trajectories because of differences in tumor visualization capabilities. In Fig. 3, T2w Spectral Presaturation with Inversion Recovery (SPIR) UQ 4D-MRI provided comparable ITV volumes to 4D CT (10.0 vs 9.3 cm³), although notable differences in spatial coverage were observed, particularly in the anterior-posterior direction. Insufficient tumor-to-liver contrast on 4D CT led to unreliable ITV estimation. In Fig. 4, T2w SPIR UQ 4D-MRI revealed a larger ITV discrepancy with 4D CT (9.8 vs 3.6 cm³), mainly because of tumor invisibility on CT images. The fat-suppressed T2w SPIR 4D-MRI enhanced tumor visualization, enabling a more accurate motion trajectory compared with 4D CT. Figure 5 demonstrates 3 representative cases comparing ITV_{4D} with conventional margin expansion approaches (ITV2 mm and ITV5 mm). Overall, ITV2 mm and ITV5 mm either overestimated or failed to adequately cover the actual tumor motion trajectory captured by ITV_{4D}. These discrepancies demonstrate that uniform margin expansion may not appropriately account for the anisotropic nature of respiratory motion, potentially leading to unnecessary normal tissue irradiation while risking inadequate target coverage in motion trajectory regions.

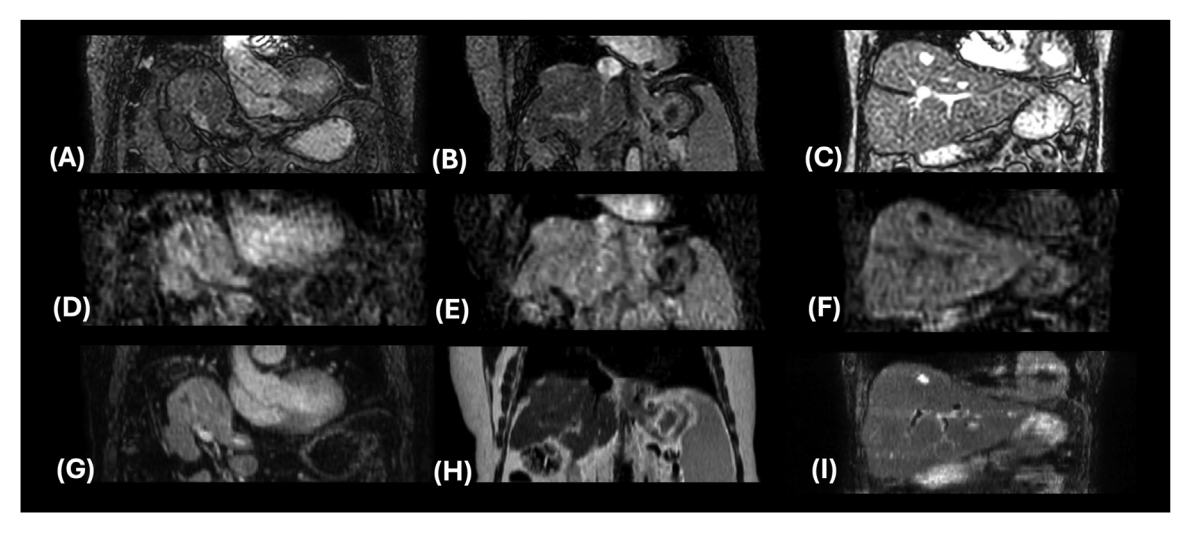


Figure 1 Coronal view of the balanced fast-field echo (A-C), 4D-THRIVE (D-F), and ultraquality 4-dimensional magnetic resonance imaging (G: T1-weighted, H: T2-weighted, and I: T2-weighted-spectral presaturation with inversion recovery) at the same phase of respiratory cycle in 3 representative patients. Ultraquality 4-dimensional magnetic resonance imaging carries respiratory motion information while providing optimal tissue contrast for different tumor types.

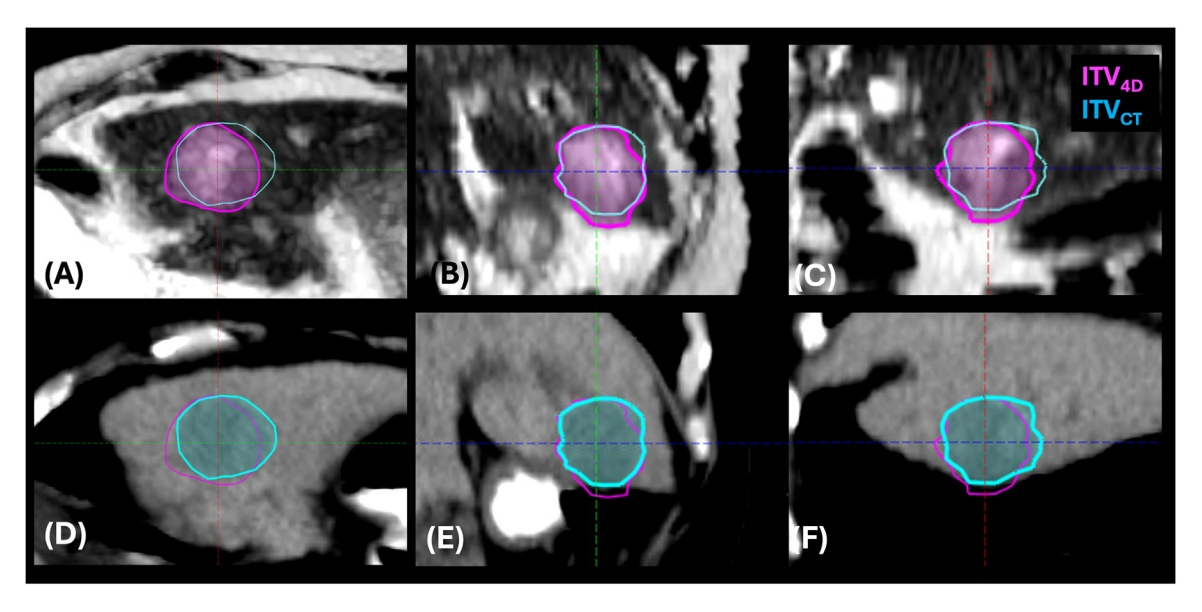


Figure 2 Internal target volume delineation comparison between T2-weighted ultraquality 4-dimensional magnetic resonance imaging (A-C) and computed tomography (D-F) shown in axial, sagittal, and coronal views for patient 4. ITV $_{4D}$ (purple) and ITV $_{CT}$ (cyan) contours demonstrate similar total volumes (17.1 vs 17.4 cm 3) but exhibit spatial discrepancies in their coverage patterns. Despite equivalent volumes, the superior soft tissue contrast of T2-weighted 4-dimensional magnetic resonance imaging reveals distinct target motion trajectories compared with 4-dimensional computed tomography. *Abbreviation*: ITV $_{CT}$ = CT-based ITV.

Discussion

This study evaluated the accuracy of UQ 4D-MRI technique for ITV estimation, which is essential for precise radiation beam delivery to a moving target. Main findings include: (1) clinical available 4D THRIVE sequence provided accurate motion delineation; (2) motion-induced liver

deformation derived from 4D THRIVE can be mapped onto the high spatial resolution 3-dimensional MRI to form UQ 4D-MRI for ITV delineation, which reduced the ITV volume compared with the isotropic margin expansion; and (3) a workflow was established to streamline image processing and implement clinical procedures for estimating ITV from 4D-MRI in treatment planning.

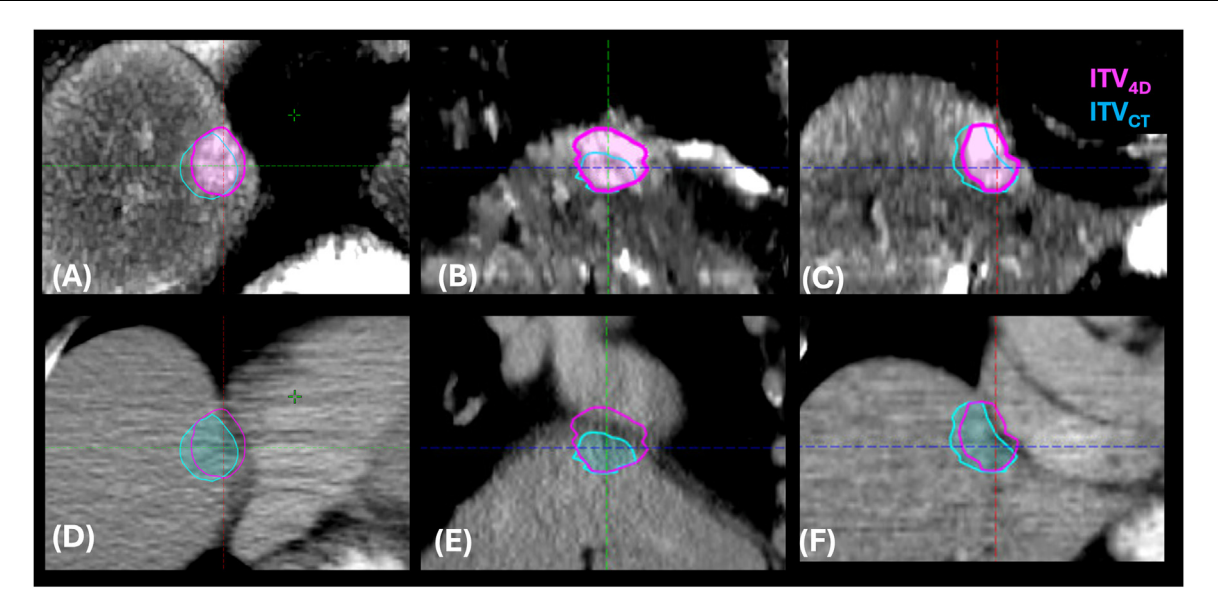


Figure 3 Internal target volume delineation comparison between T2-weighted spectral presaturation with inversion recovery ultraquality 4-dimensional magnetic resonance imaging (A-C) and computed tomography (D-F) shown in axial, sagittal, and coronal views for patient 11. ITV_{4D} (purple) and ITV_{CT} (cyan) contours show comparable total volumes (10.0 vs 9.3 cm 3) with distinct delineation patterns. The tumor cannot be clearly identified on the 4-dimensional computed tomography images. The fat-suppressed T2-weighted spectral presaturation with inversion recovery computed tomography images provide enhanced tumor visualization against surrounding tissue, revealing spatial differences in target motion coverage, particularly noticeable in the sagittal and coronal planes.

Abbreviation: $ITV_{CT} = CT$ -based ITV.

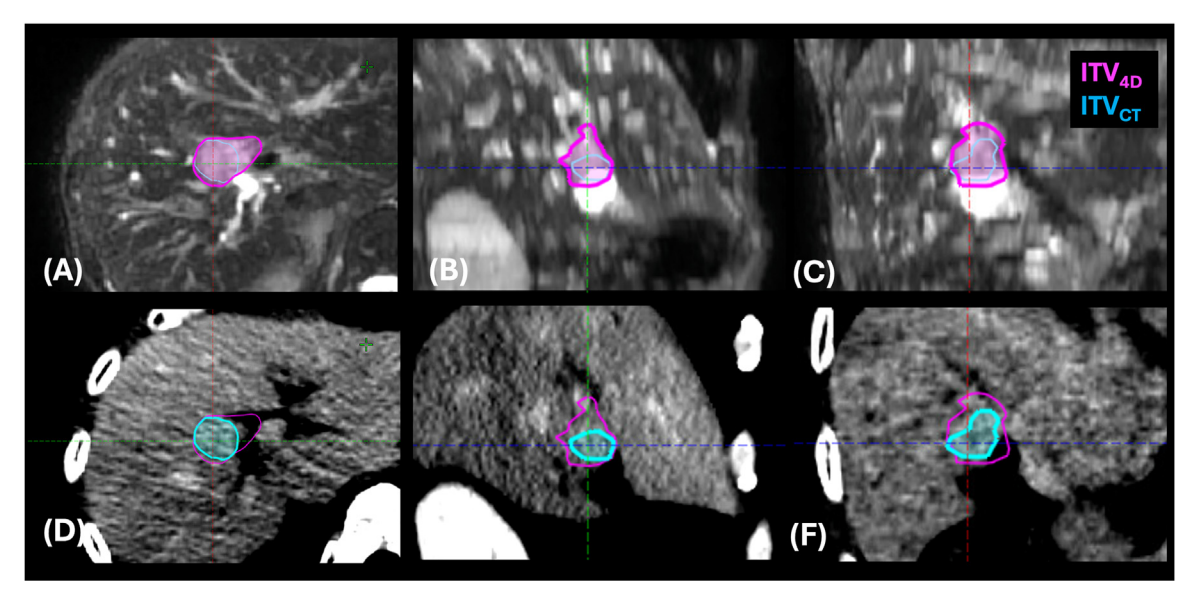


Figure 4 Internal target volume delineation comparison between T2-weighted spectral presaturation with inversion recovery ultraquality 4-dimensional magnetic resonance imaging (A-C) and computed tomography (D-F) shown in axial, sagittal, and coronal views for patient 7. ITV_{4D} (purple) and ITV_{CT} (cyan) contours show large volume differences (9.8 vs 3.6 cm³), mainly because of invisibility of the tumor on computed tomography images. The fat-suppressed T2-weighted spectral presaturation with inversion recovery 4-dimensional images reveal enhanced tumor visualization and more accurate motion trajectory compared to 4-dimensional computed tomography. Abbreviation: $ITV_{CT} = CT$ -based ITV.

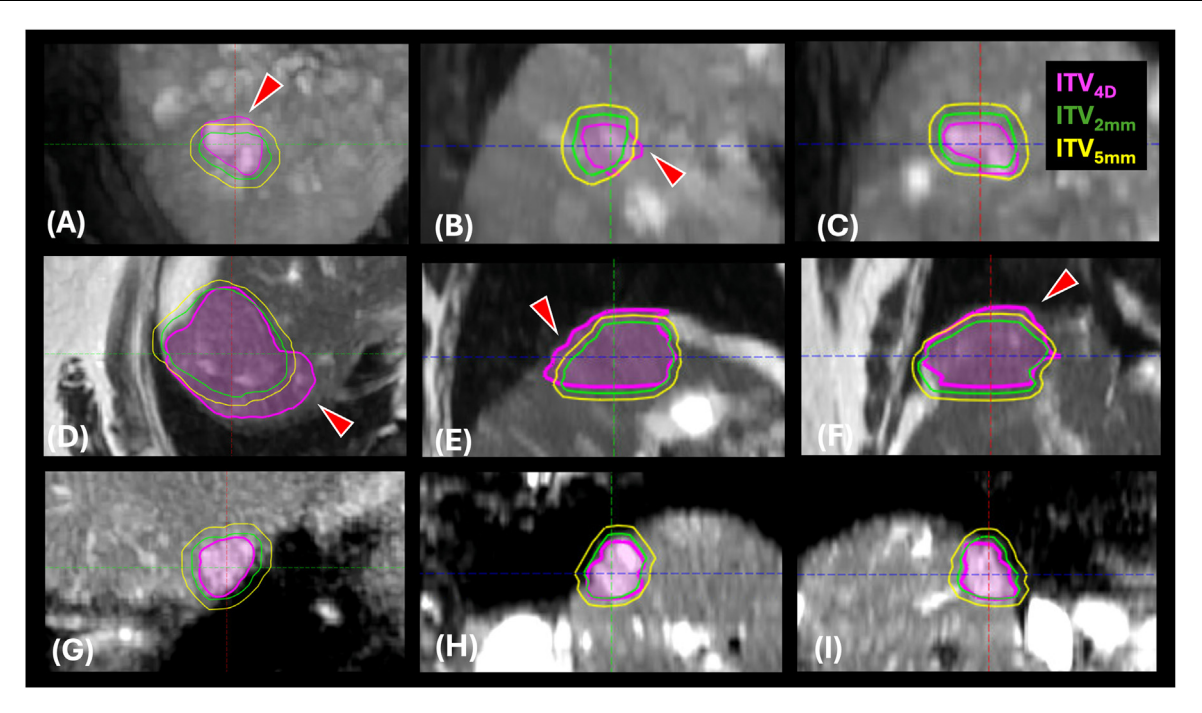


Figure 5 Comparison of internal target volume delineation methods based on ultraquality 4-dimensional magnetic resonance imaging versus traditional expansion approaches in 3 representative patients (patients 2, 6, and 12), shown in each row in axial, sagittal, and coronal views. ITV_{4D} (purple), $ITV_{2\ mm}$ (green), and $ITV_{5\ mm}$ (yellow) are overlaid on ultraquality T1-weighted (A-C), T2-weighted (D-F), and T2-weighted-spectral presaturation with inversion recovery (G-I) magnetic resonance imaging. Red arrowheads indicate regions with significant discrepancies between ITV_{4D} and the isotropic expansion methods ($ITV_{2\ mm}$ and $ITV_{5\ mm}$), illustrating potential areas of over- or under-estimation of tumor motion coverage using traditional approaches.

Accounting for respiratory motion is necessary to generate accurate dosimetry plans when treating tumors in the abdomen, particularly in stereotactic body RT. Currently, there are 2 main approaches in clinical practice: using 4D-CT for respiratory motion assessment and ITV definition or directly applying empirical margins to the GTV. In our routine 4D-CT protocol, 3 phases (0%, 50%, and 90%) from the 4D-CT are used to define ITV_{CT}, either through direct contouring on CT when tumors are visible or MRI-CT fusion when tumors are better visualized on MRI. Alternatively, some clinical practices apply standardized uniform margins (commonly 2-5 mm) to GTV, accounting for respiratory motion, particularly when motion assessment is challenging.

With the increased use of MRI in RT simulation because of its superior soft tissue contrast, respiratory-correlated 4D-MRI is highly desired for target motion assessment. However, most 4D-MRI techniques require specially designed MR sequences with sparsely undersampled acquisition strategies and complicated image reconstruction methods, which has greatly hindered the clinical implementation of 4D-MRI. Our study demonstrated the clinical deployment of a UQ 4D-MRI method that complements current planning approaches. This approach generates 4D-MRI from commercially available MR sequences by including a 1-minute 4D THRIVE scan to the standard MR-Sim protocol. The UQ 4D-MRI is

generated by deforming high-quality 3-dimensional images with the DVF derived from the low-resolution 4D THRIVE scan. Because our standard clinical protocol includes various tissue contrasts using different 3-dimensional MRI sequences (T1w, T2w, fat-saturated, and dynamic contrast-enhanced MRI, etc.), UQ 4D-MRI can be generated based on any of these sequences. This flexibility indicates that UQ 4D-MRI could improve liver tumor RT planning without increasing the examination time of our routine MR-Sim clinical protocol.

The phantom validation study demonstrated excellent agreement between 4D-THRIVE and reference 2-dimensional bFFE measurements across various motion conditions (peak-to-peak displacements of 10, 20, and 30 mm with respiratory periods of 4, 6, 8, and 12 seconds). This validated the reliability of 4D-THRIVE's motion detection capability, which serves as the foundation for UQ 4D-MRI reconstruction. Although the phantom represents rigid motion different from deformable tumor movement, the consistent motion tracking accuracy supported using 4D-THRIVE-derived deformation fields for high-quality UQ 4D-MRI generation.

In clinical validation, although ITV_{4D} volumes showed no significant differences from current clinical standard ITV_{CT} (average, 12.4 vs 12.6 cm³; P = .72), UQ 4D-MRl's superior soft tissue contrast enables more precise tumor motion trajectory estimation compared with 4D-CT.

When comparing to conventional uniform margin expansion approaches, ITV $_{2~\mathrm{mm}}$ and ITV $_{5~\mathrm{mm}}$ significantly overestimated target volumes by 29.0% (P = .002) and 120.7% (P < .0001), respectively. While these uniform expansions generally encompassed the tumor motion range, they do not account for anisotropic motion and organ deformation. This limitation may lead to unnecessary normal tissue irradiation while risking inadequate target coverage. Furthermore, the successful implementation of UQ 4D-MRI for motion assessment plays an important role in supporting MR-only simulation workflow, potentially eliminating the need for CT-Sim.

This study has several limitations. First, by using singleslice high temporal resolution 2-dimensional bFFE as the gold standard, different tumor locations and appearances in this imaging make the comparison with UQ 4D-MRI in the tumor area not ideal, necessitating the selection of another anatomic landmark close to the tumor (eg, blood vessels and organ edges) for displacement measurements. Second, a patient's breathing pattern during MR-Sim does not always replicate that during radiation delivery, highlighting the importance of systematic respiratory management techniques. These include the use of compression devices and respiratory monitors to ensure ITV reproducibility or acquiring 4D-MRI immediately before radiation delivery to verify ITV. Third, the spatial resolution of 4D THRIVE, being $3 \times 3 \times 3$ mm³, presented challenges in detecting tumor movement ranges smaller than 3 mm. The average maximum diaphragm displacement of 5.2 mm among 13 patients in this study only approximately corresponded to 2 slices of displacement in the UQ 4D-MRI. Lastly, ITV in our study was extended based on GTV rather than CTV, resulting in an ITV slightly smaller than that defined byInternational Commission on Radiation Units and Measurements (ICRU) Report 62.3 Nonetheless, comparing GTV-expanded and CTV-expanded ITV is out of the scope of this study. The same method used in this study can be readily transferred to CTV-expanded ITV. Lastly, the UQ 4D-MRI dual-supervised deformation estimation model used in this study cannot be directly applied to other body parts such as the kidney and chest. Future studies will focus on expanding the generalizability of the model to ensure consistent and reliable results across diverse data sets and conditions.

In conclusion, this study validated the accuracy of UQ 4D-MRI in liver tumor motion measurement during MR-Sim, critical for estimating the accurate margin of ITV in radiation treatment planning. We successfully deployed the UQ 4D-MRI protocol in our clinical practice by adding only a 1-minute commercially available 4D THRIVE sequence to our standard examination protocol. This workflow improves physicians' confidence in target motion assessment and ITV delineation, offering the potential to reduce PTV margin and streamline MR-RT planning in patients with upper gastrointestinal cancer. The ability to achieve a more precise ITV definition could

enhance the sparing of critical organs, including normal liver, stomach, and duodenum, while ensuring optimal target coverage. This advancement offers the potential to reduce PTV margins and streamline MR-guided-RT planning for patients with upper gastrointestinal cancer.

Disclosures

The authors declare that they have no known competing financial interests or personal relationships that could have appeared to influence the work reported in this paper.

Supplementary materials

Supplementary material associated with this article can be found in the online version at doi:10.1016/j.adro.2025.101774.

References

- Teh B. Image-guided stereotactic body radiation therapy (SBRT):
 An emerging treatment paradigm with a new promise in radiation oncology. Biomed Imaging Interv J. 2007;3:e5.
- Kishan AU, Ma TM, Lamb JM, et al. Magnetic resonance imagingguided vs computed tomography-guided stereotactic body radiotherapy for prostate cancer: The MIRAGE randomized clinical trial. *JAMA Oncol.* 2023;9:365-373.
- International Commission on Radiation Units and Measurements, ICRU Report 62: Prescribing, recording and reporting photon beam therapy (supplement to ICRU Report 50). Volume os-32. November 1999
- Li R, Han B, Meng B, et al. Clinical implementation of intrafraction cone beam computed tomography imaging during lung tumor stereotactic ablative radiation therapy. *Int J Radiat Oncol Biol Phys.* 2013;87:917-923.
- Lacornerie T, Lisbona A, Mirabel X, Lartigau E, Reynaert N. GTVbased prescription in SBRT for lung lesions using advanced dose calculation algorithms. *Radiat Oncol.* 2014;9:223.
- Wang Y, Liu T, Chen H, Bai P, Zhan Q, Liang X. Comparison of internal target volumes defined by three-dimensional, four-dimensional, and cone-beam computed tomography images of a motion phantom. *Ann Transl Med.* 2020;8:1488.
- Han-Oh S, Hill C, Kang-Hsin Wang K, et al. Geometric reproducibility
 of fiducial markers and efficacy of a patient-specific margin design
 using deep inspiration breath hold for stereotactic body radiation therapy for pancreatic cancer. Adv Radiat Oncol. 2021;6:100655.
- Nitta Y, Ueda Y, Murata S, et al. Setup accuracy and dose attenuation of a wooden immobilization system for lung stereotactic body radiotherapy. Rep Pract Oncol Radiother. 2022;27:809-820.
- Dang HQ, Nguyen CT, Pham HV, et al. The institutional experience of the implementing 4DCT in NSCLC radiotherapy planning. Rep Pract Oncol Radiother. 2023;28:445-453.
- Tryggestad E, Li H, Rong Y. 4DCT is long overdue for improvement. J Appl Clin Med Phys. 2023;24:e13933.
- Río Bártulos C, Senk K, Schumacher M, et al. Assessment of liver function with MRI: Where do we stand? Front Med (Lausanne). 2022;9:839919.
- Cai J, Chang Z, Wang Z, Paul Segars W, Yin FF. Four-dimensional magnetic resonance imaging (4D-MRI) using image-based respiratory surrogate: A feasibility study. *Med Phys.* 2011;38:6384-6394.

- Liu Y, Yin FF, Czito BG, Bashir MR, Cai J. T2-weighted four dimensional magnetic resonance imaging with result-driven phase sorting. *Med Phys.* 2015;42:4460-4471.
- Liu Y, Zhong X, Czito BG, et al. Four-dimensional diffusionweighted MR imaging (4D-DWI): A feasibility study. *Med Phys.* 2017;44(2):397-406.
- Stemkens B, Paulson ES, Tijssen RHN. Nuts and bolts of 4D-MRI for radiotherapy. Phys Med Biol. 2018;63:21TR01.
- Wang C, Yin FF. 4D-MRI in radiotherapy [Internet]. Magnetic resonance imaging. IntechOpen; 2019.
- Yang J, Cai J, Wang H, et al. Four-dimensional magnetic resonance imaging using axial body area as respiratory surrogate: Initial patient results. Int J Radiat Oncol Biol Phys. 2014;88:907-912.
- Liu Y, Yin FF, Chen NK, Chu ML, Cai J. Four dimensional magnetic resonance imaging with retrospective k-space reordering: A feasibility study. Med Phys. 2015;42:534-541.
- 19. Liang X, Yin FF, Liu Y, Cai J. A probability-based multi-cycle sorting method for 4D-MRI: A simulation study. *Med Phys.* 2016;43:6375.
- Li T, Cui D, Hui ES, Cai J. Time-resolved magnetic resonance fingerprinting for radiotherapy motion management. *Med Phys*. 2020;47:6286-6293. Erratum in: *Med Phys*. 2021;48:2698.
- Li G, Wei J, Olek D, et al. Direct comparison of respiration-correlated four-dimensional magnetic resonance imaging reconstructed using concurrent internal navigator and external bellows. *Int J Radiat Oncol Biol Phys.* 2017;97:596-605.
- Yuan J, Wong OL, Zhou Y, Chueng KY, Yu SK. A fast volumetric 4D-MRI with sub-second frame rate for abdominal motion monitoring and characterization in MRI-guided radiotherapy. Quant Imaging Med Surg. 2019;9:1303-1314.
- Feng L. Live-view 4D GRASP MRI: A framework for robust realtime respiratory motion tracking with a sub-second imaging latency. *Magn Reson Med.* 2023;90:1053-1068.

- 24. Li G, Sun A, Nie X, et al. Introduction of a pseudo demons force to enhance deformation range for robust reconstruction of super-resolution time-resolved 4DMRI. *Med Phys.* 2018;45:5197-5207.
- 25. Li G, Wei J, Kadbi M, et al. Novel super-resolution approach to time-resolved volumetric 4-dimensional magnetic resonance imaging with high spatiotemporal resolution for multi-breathing cycle motion assessment. *Int J Radiat Oncol Biol Phys.* 2017;98:454-462.
- Harris W, Ren L, Cai J, Zhang Y, Chang Z, Yin FF. A technique for generating volumetric cine-magnetic resonance imaging. *Int J Radiat Oncol Biol Phys.* 2016;95:844-853.
- Terpstra ML, Maspero M, Verhoeff JJC, van den Berg CAT. Accelerated respiratory-resolved 4D-MRI with separable spatio-temporal neural networks. *Med Phys.* 2023;50:5331-5342.
- 28. Xiao H, Han X, Zhi S, et al. Ultra-fast multi-parametric 4D-MRI image reconstruction for real-time applications using a downsampling-invariant deformable registration (D2R) model. *Radiother Oncol.* 2023;189:109948.
- Zhi S, Wang Y, Xiao H, et al. Coarse-super-resolution-fine network (CoSF-Net): A unified end-to-end neural network for 4D-MRI with simultaneous motion estimation and super-resolution. *IEEE Trans Med Imaging*. 2024;43:162-174.
- Xiao H, Ni R, Zhi S, et al. A dual-supervised deformation estimation model (DDEM) for constructing ultra-quality 4D-MRI based on a commercial low-quality 4D-MRI for liver cancer radiation therapy. *Med Phys.* 2022;49:3159-3170.
- Glide-Hurst CK, Paulson ES, McGee K, et al. Task group 284 report: Magnetic resonance imaging simulation in radiotherapy: Considerations for clinical implementation, optimization, and quality assurance. *Med Phys.* 2021;48:e636-e670.
- **32.** Mengler L, Khmelinskii A, Diedenhofen M, et al. Brain maturation of the adolescent rat cortex and striatum: Changes in volume and myelination. *Neuroimage*. 2014;84:35-44.